Respiratory Physiology & Neurobiology 185 (2013) 647–652

Contents lists available at SciVerse ScienceDirect

Respiratory Physiology & Neurobiology

journal homepage: www.elsevier.com/locate/resphysiol

Dynamics of gas micronuclei formed on a flat hydrophobic surface, the predecessors of decompression bubbles

R. Arieli[a,*], A. Marmur[b]

[a] Israel Naval Medical Institute, IDF Medical Corps, Haifa, Israel
[b] Department of Chemical Engineering, Technion-Israel Institute of Technology, Haifa, Israel

ARTICLE INFO

Article history:
Accepted 30 November 2012

Keywords:
Nanobubble
Hyperbaric pressure
Silicon wafer

ABSTRACT

It is a long-standing hypothesis that the bubbles which evolve as a result of decompression have their origin in stable gas micronuclei. In a previous study (Arieli and Marmur, 2011), we used hydrophilic and monolayer-covered hydrophobic smooth silicon wafers to show that nanobubbles formed on a flat hydrophobic surface may be the gas micronuclei responsible for the bubbles that evolve to cause decompression sickness. On decompression, bubbles appeared only on the hydrophobic wafers. The purpose of the present study was to examine the dynamics of bubble evolution. The numbers of bubbles after decompression were greater with increasing hydrophobicity. Bubbles appeared after decompression from 150 kPa, and their density increased with elevation of the exposure pressure (and supersaturation), up to 400 kPa. The normal force of attraction between the hydrophobic surface and the bubble, as determined from the volume of bubbles leaving the surface of the wafer, was 38×10^{-5} N and the tangential force was 20×10^{-5} N. We discuss the correlation of these results with previous reports of experimental decompression and bubble formation, and suggest to consider appropriate modification of decompression models.

1. Introduction

One of the main limitations on diving is decompression sickness (DCS), which is caused by the evolution of bubbles in tissue supersaturated with inert gases following decompression from high pressure. For a bubble to evolve, a critical (minimal) size is required to start the process. Bubbles smaller than this critical size redissolve, due to the high pressure caused by surface tension. Thus, as is now widely known, nuclei having a critical radius of curvature must be present before or during decompression for bubbles to evolve in a diver (Hennessy, 1989).

Over the last half a century, it was proposed, for example, that gas micronuclei are formed by cavitation, when two solid surfaces in a liquid are separated (Craig, 1996; Hayward, 1967). It has been suggested that these nuclei are stable gas micronuclei that are present in hydrophobic crevices (Harvey et al., 1944; Liebermann, 1957), or that they are enclosed in micelles of surface-active molecules (Fox and Herzfeld, 1954; Yount et al., 1977). We recently argued that gas micronuclei might be formed in the human body on flat hydrophobic surface that do not have crevices (Arieli and Marmur, 2011). This is so, since it has been shown, using atomic force microscopy, that tiny, flat gas nanobubbles, measuring 5–30 nm, form spontaneously when a smooth (almost uni-molecular) hydrophobic surface is submerged in water containing dissolved gas (Meyer et al., 2005; Singh et al., 2006; Stevens et al., 2005; Switkes and Ruberti, 2004; Tyrrell and Attard, 2001; Yang et al., 2007). While the existence of nanobubbles on hydrophobic surfaces is generally accepted, the mechanism responsible for their stability is yet under discussion (Seddon et al., 2011; Weijs et al., 2012).

In our previous study (Arieli and Marmur, 2011), these nanobubbles were assumed to be the source of gas micronuclei from which bubbles evolved during decompression on smooth hydrophobic wafers. Indeed, bubbles evolved on hydrophobic but not hydrophilic, silicon wafers. This publication also dealt extensively with a possible critique of the method, to the effect that air cavities may have been produced on insertion of the wafer into the water. The main arguments against this were that (a) large numbers of studies had failed to observe any bubbles or nanobubbles on hydrophobic wafers placed in water, following degassing at low pressures (below 10 kPa, which is above our degassing pressure); and (b) no nanobubbles were present when wafers were placed in ethanol, while they appeared after anaerobic replacement of the ethanol with water (Considine et al., 1999; Meyer et al., 2005; Stevens et al., 2005; Switkes and Ruberti, 2004, among others).

There are numerous hydrophobic surfaces in the living body, such as subcutaneous fat, visceral fat, and part of the inner surface of

* Corresponding author at: Israel Naval Medical Institute, P.O. Box 8040, 31080 Haifa, Israel. Tel.: +972 77 8100825; fax: +972 4 9801210.
E-mail address: rarieli@netvision.net.il (R. Arieli).

1569-9048/$ – see front matter © 2012 Elsevier B.V. All rights reserved.
http://dx.doi.org/10.1016/j.resp.2012.11.020

blood cavities: the umbilical vein, right ventricle, pulmonary vein, and left ventricle (Hills, 1992). Hills (1992) also demonstrated an oligolamellar lining of phospholipids on the luminal aspect of many blood vessels: venules and capillaries in the cerebral cortex and the aortic endothelium. These surfaces may be the sites where gas micronuclei form spontaneously, even in the absence of crevices.

To further the understanding of decompression-induced bubble evolution, the present paper focuses on the following essential questions: (1) Do the effective gas micronuclei depend on the level of gas supersaturation? Effective gas micronuclei are the subpopulation of nanobubbles that were transformed to growing bubbles. (2) What is the force required to detach a bubble from the surface at which it originated? (3) What is the time scale for the evolution of gas micronuclei? These questions were experimentally studied, using well-defined, hydrophilic and hydrophobized silicon wafers.

2. Methods

2.1. Wafer preparation

Silicon wafers are almost molecularly flat with no crevices on their surface. Circular silicon wafers from two sources, 100 mm P/B(100) 1–10 Ω cm 500 μm (SSP Prime, University Wafer, Boston, MA), henceforth designated UW-wafers, and 100 mm P/B/Cz 10–20 Ω cm 500 μm (Semiconductor Processing Co., Boston, MA), designated SP-wafers. In our previous study (Arieli and Marmur, 2011) we used UW wafers. Report from the experience in the laboratory pointed that hydrophobicity of UW wafers was lower than that of SP wafers. This led us to choose both for the study of the effect of the level of hydrophobicity. Wafers were cut into squares with sides measuring 4.5–5.0 cm. Wafers were cleaned, coated with a hydrophobic layer and the advancing and receding contact angles (as a measure of hydrophobicity) were done as described in our previous paper (Arieli and Marmur, 2011). The hydrophobic molecules bind covalently to the wafer and therefore produce uni-molecular coating. After a few hyperbaric exposures the wafers lost some of their hydrophobicity, probably due to their becoming contaminated or oxidized. This was suspected when bubble density in a used set of wafers was lower than in freshly added wafer, and was later confirmed by measurement of the contact angle. We therefore used more than one batch of wafers, designated UW-I and UW-II, and SP-I, SP-II and SP-III. The contact angles of the hydrophobic UW-I-wafers with a drop of water were $109.8 \pm 2.1^\circ$ for advancing angle, $78.7 \pm 4.5^\circ$ for receding angle, and hysteresis (advancing minus receding angle) $31.1 \pm 4.7^\circ$; contact angles of UW-II-wafers were $115.3 \pm 1.1^\circ$ for advancing angle, $95.4 \pm 2.1^\circ$ for receding angle, and hysteresis $19.9 \pm 1.6^\circ$. Advancing angle of UW-II was greater than UW-I (t-test, $P < 0.002$), and hysteresis of UW-II was lower than UW-I (t-test, $P < 0.005$). There was no significant difference in advancing contact angle between the three hydrophobic SP batches ($113.8 \pm 1.5^\circ$, $114.0 \pm 1.4^\circ$, and $115.1 \pm 1.7^\circ$ for SP-I, SP-II and SP-III, respectively). Hysteresis was $13.4 \pm 1.5^\circ$, $13.0 \pm 1.2^\circ$, and $17.6 \pm 1.6^\circ$ for SP-I, SP-II and SP-III, respectively; hysteresis of SP-III was significantly higher than SP-II and SP-I (ANOVA, $P < 0.009$). An overall comparison of SP- and UW-wafers yielded no significant difference in advancing angle, but higher hysteresis for UW-wafers (t-test, $P < 0.0001$). Each batch consisted of 6–7 wafers, with a total area of 145 ± 7 cm^2. A few clean wafers were left without the coating to serve as a hydrophilic reference (contact angle $\sim 30^\circ$).

2.2. Degassing and hyperbaric exposure

A Pyrex bowl (diameter 26 cm, height 5 cm) was filled with double distilled water (18 MΩ) to a level of 3 cm, and placed for a day in a desiccator (Vacuum pump XDS 5, Edwards, Crawley, West Sussex, UK) at a low pressure of 3.2–3.8 kPa, about 1 kPa above water vapor pressure, for washout of dissolved gases and any tiny bubbles. Ambient (room) pressure was restored, and the silicon wafers (6–7 hydrophobic and 1 hydrophilic) were rinsed with double distilled water and placed under the water with the shiny, almost molecularly flat surface facing upward. Low pressure was resumed for another 1 h, after which ambient pressure was again restored. The few bubbles which appeared on the hydrophobic wafers during the low pressure phase were released by tapping on the desiccator. The wafers were left underwater in the desiccator at ambient pressure and exposed to the surrounding air for 2 h (unless as specified in Protocol III). This time was allowed for the assumed formation of nanobubbles on the hydrophobic surfaces from the dissolved air.

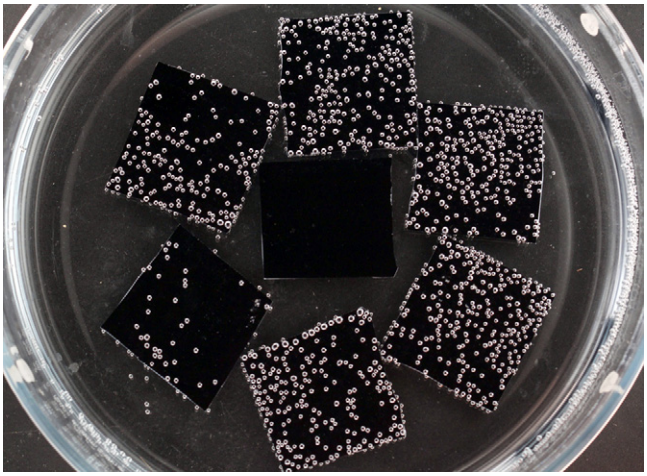

Fig. 1. Six hydrophobic UW-I-wafers on the periphery and one hydrophilic UW-I-wafer in the center, photographed 2.5 h after decompression from 300 kPa (20 msw).

The bowl was then transferred from the desiccator to a 150-l hyperbaric chamber (Roberto Galeazzi, La Spezia, Italy), a ribbon of chromatographic paper was pasted around the rim, and it was covered with another glass bowl to prevent dust contamination. The bowl containing the wafers was kept at the scheduled pressure for 20 h, at room temperature. The pressure was then reduced at 100 kPa/min to that of the surface (the ambient pressure in the room). The bowl was carefully removed from the hyperbaric chamber for photography. At the end of the photographic session, the wafers were rinsed with double distilled water and left out to dry under cover on filter paper before storage for the next experiment. The glass bowls were dried and then rinsed, first with propanol and then acetone; the desiccator was also rinsed, first with propanol and then ethanol. A photograph of one batch of UW-wafers is shown in Fig. 1. These wafers were photographed 2.5 h after decompression, when the bubbles had reached a volume that enabled us to see a clear contrast. As has already been shown in our previous report (Arieli and Marmur, 2011), no bubbles evolved on the hydrophilic wafer in the center of the bowl, but only on the hydrophobic wafers in the periphery. Hydrophilic wafers were therefore of no further concern. All procedures were conducted at a room temperature of 19–24 °C.

2.3. Experimental protocols

2.3.1. Protocol I: effect of hyperbaric pressure (gas supersaturation) on the density of gas micronuclei

Hyperbaric pressures at 50 kPa (5 msw) intervals between 150 kPa (5 msw) and 400 kPa (30 msw) were selected in random order. The bubbles which formed on each wafer were photographed immediately (1–5 min) after decompression. Bubbles were counted using an image processing program (Image-Pro-Plus, Media

Fig. 2. Side view of a hydrophobic UW-I-wafer with brass weights photographed 1.5 h after decompression. At that time, a large number of bubbles floated to the water surface. Bubbles are spherical in shape, with reflections of other small bubbles and a mirror image from the smooth surface of the wafer.

Cybernetics Inc., Bethesda, MD). Bubble density was calculated by dividing the total number of bubbles counted for each wafer by its surface area. The actual pressure after overnight stabilization was not the exact initial pressure, but diverged by 10–20 cm of seawater. The low pressure employed for degassing was 3.8 ± 0.5 kPa, and the procedure lasted 23 ± 2 h. Exposure to hyperbaric pressure lasted 20 ± 1 h, and temperature before decompression was 19–25 °C for the UW1-wafers and 22–25 °C for SP-wafers.

2.3.2. Protocol II: bubble-hydrophobic surface attraction force

Protocol IIa: normal attraction force. After placing the wafers on the bottom of the bowl, two brass weights were positioned on opposite edges of each wafer to prevent it from floating up to the surface due to the increasing volume of the bubbles. Hyperbaric exposure was set at 1010 kPa (90 msw), which ensured a high level of supersaturation that would not limit bubble growth. Following decompression, wafers were photographed at 5-min intervals over a period of 4 h. A 5-min interval was chosen because the diameter of a bubble growing for 5 min would be below our selected measurement precision of 0.2 mm. Bubbles could be followed easily from the start as a small dot, as they grew, and eventually coalesced with other bubbles. Sequences of two photographs were compared to select bubbles which floated to the surface. After the release of a bubble, a number of new bubbles nucleated on the site it had previously occupied. Care was taken to consider only first generation bubbles, because as the new generation of small bubbles appeared it would take time for their growth with diminishing dissolved gas and therefore most of the next generation bubbles would not reach detachment size. The diameter of a bubble was measured just before it floated up toward the surface, making use of the wafer width as a reference. For calculation of the buoyancy force the bubble was assumed to be spherical, as may be seen from a side view of bubbles close to floating size (Fig. 2). The volume (weight) of water displaced by the bubble was assumed to be the upward force on detachment.

Protocol IIb: tangential attraction force. This was similar to the protocol for the normal attraction force, except that the hydrophobic wafers were placed vertically in two slits carved in a Plexiglas plate placed on the bottom of a TLC glass Developing Tank measuring 9.5 cm × 19 cm × 17 cm. Wafers were photographed through the walls of the tank. Tests were done for alignments with both UW-wafers and SP-wafers. Exposure to hyperbaric pressure lasted 21 ± 2 h, and temperature at the end of the exposure was 22 ± 2 °C.

2.3.3. Protocol III: time for formation of gas micronuclei

This protocol was aimed to find how long it takes for nanobubbles (and gas micronuclei) to be present on a wafer which was initially without nanobubbles. Wafers in water under very low pressure were considered to have no nanobubbles. If it takes some definite period for the appearance of nanobubbles, adding supersaturated water to the degassed wafers before this definite period, would not result in bubble formation, but bubbles will evolve if supersaturated water is added after this period. A plastic container with a tap on the bottom was partly filled with double distilled water and placed in the hyperbaric chamber at 300 kPa for at least 24 h. At the same time, the degassing procedure was conducted with a water level of only 1 cm; wafers were placed in the bowl 1 h before the end of degassing. We allowed different periods of time to intervene between the end of degassing and the release of high pressure for removal of the plastic container from the hyperbaric chamber (starting from the shortest time possible), before carefully adding the supersaturated water to the wafers in the bowl at ambient pressure. The tap of the supersaturated plastic container was dipped into the water in the glass bowl, and the flow of the water was kept low, ~80 ml/min, to limit turbulence and bubble formation. Wafers were photographed immediately after that.

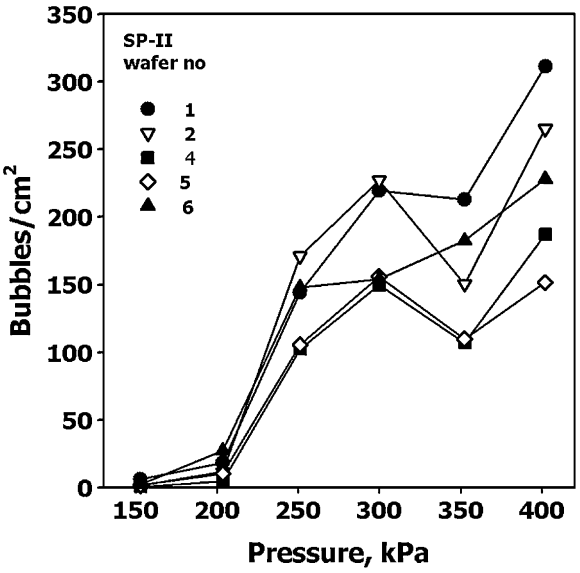

Fig. 3. The difference between wafers is exemplified by the bubble density immediately after decompression of 5 selected hydrophobic SP-II-wafers as a function of the value pressure reached before decompression.

2.4. Statistical analysis

Data regarding contact angles (advancing and hysteresis) and bubble size on detachment were tested for normality by the Kolmogorov–Smirnov test. The groups were then compared using ANOVA and a *t*-test. Interactions and pairwise contrast were used to test the effects of exposure pressure on bubble density. The number of bubbles released as a function of time was tested using the Spearman correlation, and the difference between the bubble production of individual wafers was examined using the Dunnett T3 test.

3. Results

3.1. Protocol I: effect of hyperbaric pressure (gas supersaturation) on the density of gas micronuclei

Although each batch was prepared in the same way, there were differences between wafers in the same batch. This is exemplified in Fig. 3, where it can be seen that some wafers had high bubble density (wafers 1 and 2), some had medium density (wafer 6),

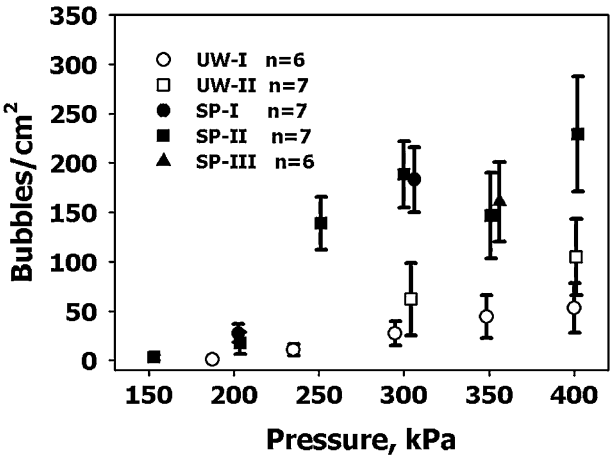

Fig. 4. Summary of the effect of hyperbaric pressure on bubble density immediately after decompression for five batches of UW- and SP-wafers (mean ± SD). Density is presented as a function of the hyperbaric pressure before the decompression.

and others had low bubble density (wafers 4 and 5). Mean bubble density is expressed in Fig. 4 as a function of the actual pressure. There was a growth in bubble density of both SP- and UW-wafers as hyperbaric pressure increased from 150 to 400 kPa (5–30 msw) ($P < 0.001$), with possible stabilization between 300 and 400 kPa in the SP-wafers. There was no difference in bubble density between the 3 batches of SP wafers. Bubble density of the SP-wafers was higher than that of the UW-wafers (Greenhouse–Geisser, $P < 0.0001$). Bubble density of the UW-I wafers was not significantly lower than that of the UW-II wafers ($P = 0.14$).

3.2. Protocol II: bubble-hydrophobic surface attraction force

Protocol IIa: normal attraction force. Bubbles grew continuously from the end of decompression until they floated to the water surface. The diameter was measured just before floating. Diameters measured over the 4-h post-decompression period are shown as a function of time for the 6 UW-I-wafers (Fig. 5). Differences can be seen between the wafers, with low-diameter bubbles released from wafer O and high-diameter bubbles from wafers A and N. This is also the reason the first bubbles released (27–37 min after decompression, Fig. 5) came from wafer O. The inequality in the size of released bubbles was significant between wafers from both batches, SP and UW (Dunnett T3 multiple comparison test). Mean diameter for

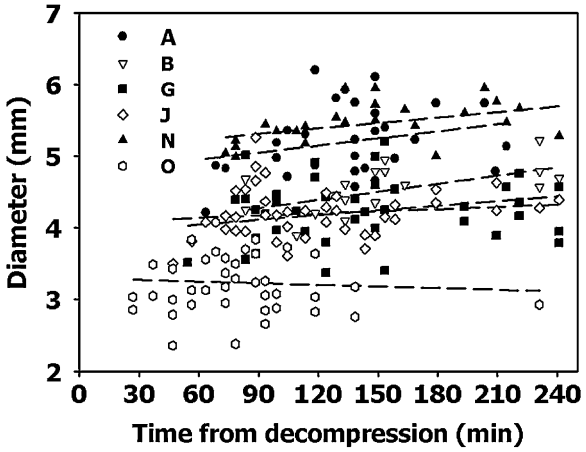

Fig. 5. Bubble diameter before detachment for 6 hydrophobic UW-I-wafers, plotted as a function of time from decompression. The different symbols represent the 6 wafers (A–O), and the regression line for each wafer is also shown (dashed lines).

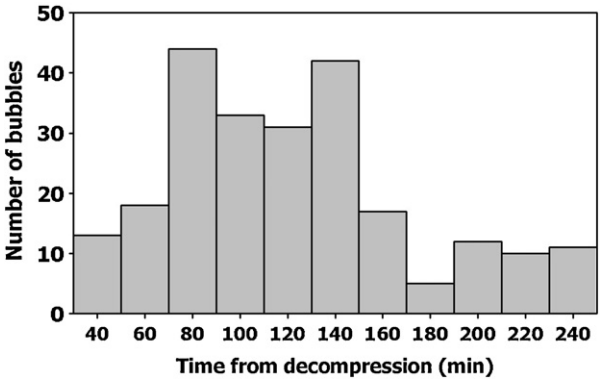

Fig. 6. Number of bubbles surfacing from 6 hydrophobic UW-I-wafers in 20-min time bins.

bubbles detaching from the wafer was 4.2 ± 0.8 mm (mean ± SD, range 2.4–5.7, $n = 262$) for UW-wafers, and 4.2 ± 0.4 mm (mean ± SD, range 3.2–6.0, $n = 130$) for SP-III-wafers. The number of bubbles in relation to surfacing time (in 20-min bins) is shown for UW-wafers in Fig. 6. Most of the first generation bubbles were released 1–2.5 h after decompression. Slopes for diameter vs. time at detachment are not different from 0, and there was therefore no time effect on bubble volume on detachment. Mean time for detachment of bubbles was 120 ± 54 min (mean ± SD) for UW-wafers, and 153 ± 61 min (mean ± SD) for SP-wafers. The estimated normal force will be considered in Section 4.

Protocol IIb: tangential attraction force. Before detachment, bubbles usually started to move vertically on the surface of the wafer. The diameter was measured before this displacement. On detachment of bubbles from the upper edge of the wafer (bubbles which had either grown on the spot, or had moved up from a lower level and stopped at the edge), the diameter was larger than when they had been on the surface of the wafer. Bubbles which became detached from the upper edge were therefore excluded. The mean diameter of bubbles released vertically from UW-wafers was 3.3 ± 0.4 mm at 127 ± 47 min after decompression, $n = 52$. For SP-wafers this was 3.5 ± 0.4 mm at 89 ± 52 min after decompression, $n = 171$. The diameter of bubbles released from the upper edge of the SP-wafers was 4.2 ± 0.5 mm, $n = 79$. The diameter of tangentially released bubbles was significantly lower than that of normally released bubbles for both SP- and UW-wafers (t-test, $P < 0.0001$). The estimated tangential force will be considered in Section 4.

3.3. Protocol III: time for formation of gas micronuclei

No difference in bubble density was found when the intervening normobaric time span was 0.1, 2, 18, and 48 h, for both UW-wafers and SP-wafers.

4. Discussion

4.1. Pressure–density

The present study shows that elevated pressure and increased gas supersaturation resulted in higher bubble density at the end of decompression. Bubbles appeared after decompression from pressure equal to or higher than 150 kPa (5 msw), and their density increased with the elevation of exposure pressure, up to 400 kPa (30 msw). It is possible that bubble density would have been even greater after exposure to pressures above 400 kPa. We did not use pressures greater than this because it was expected that as their density increased, bubbles would coalesce in the short time necessary for decompression and transfer of the bowl for photography,

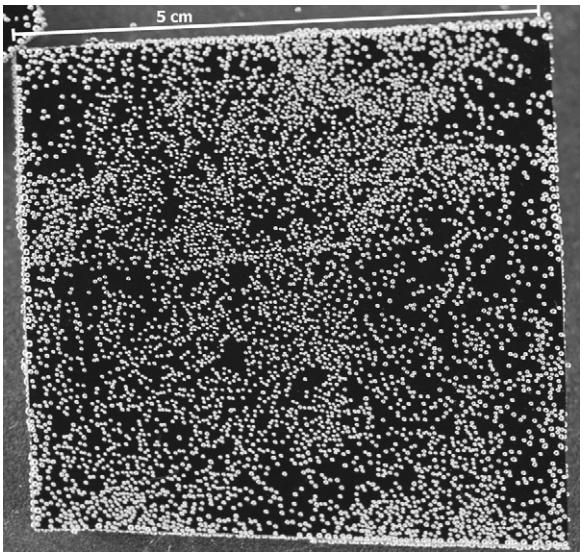

Fig. 7. Photograph of wafer 3 from SP-II, 1 min after decompression from 300 kPa. In many spots, bubbles are in close contact with one another.

and any bubble count would therefore underestimate their original density. The highest densities after decompression from 400 kPa, for 6 different SP wafers were: 216, 227, 246, 264, 279 and 311 bubbles per 1 cm^2. It is possible that initially there were even greater numbers of micronuclei, which coalesced before they became visible; this may be inferred from the close proximity of bubbles just 1 min after decompression (Fig. 7). In real life decompression, this initial coalescence might determine the highest bubble density. However, in real tissue with reduced hydrophobicity and therefore reduced bubble density, increased supersaturation may increase bubble formation.

Higher bubble density for SP-wafers compared with the UW-wafers may be related to the lower hysteresis of SP-wafers ($\Delta = 14.5^\circ$). The trend for higher bubble density for UW-II-wafers compared with UW-I-wafers may be related to the higher advancing angle (115.3° vs. 109.8°) and lower hysteresis ($\Delta = 19.9^\circ$ vs. 31.1°) of the UW-II-wafers. These two traits, high advancing angle and low hysteresis, are indicative of a better hydrophobic coating and therefore increased nucleation. The similar bubble density of SP wafers at 300, 350 and 400 kPa, may suggest either saturation of the nucleation sites, or that at high density (with very little space left between bubbles), small bubbles coalesced in the interval between decompression and photography, with the result that the measured density underestimated true nucleation.

The relationship between the level of pressure equilibration and bubble density (Figs. 3 and 4) is similar to the relationship between bubble score (according to the Kisman/Masurel code) and decompression steps (from between 135 and 190 kPa) for saturation dives in humans (Eckenhoff et al., 1990). It also agrees with studies of bubble formation in gelatin (Yount and Strauss, 1976), where higher bubble density was found with increasing decompression steps. Our study in the transparent prawn (Arieli et al., 2007) also found a higher bubble count with increasing decompression steps, reaching a 3-fold increase during decompression step from 700 kPa to 100 kPa, compared with the step from 200 kPa to 100 kPa. Seeking a possible explanation for this, Flook (Jones et al., 2007) suggested that when supersaturation is low some micronuclei do not grow to a visible size, so that low bubble density is observed after a mild hyperbaric exposure, whereas high bubble density is observed after a large decompression step when more bubbles become visible. However in the present study, when enough time was allowed in *Protocol II*, bubbles continued to grow, but no new first generation bubbles appeared. Thus, whereas extra-dissolved gas expanded to produce visible bubbles, no invisible bubbles grew to become visible. We therefore suggest that a higher pressure drop (and thus higher supersaturation) activates more nanobubbles to become gas micronuclei and form bubbles.

4.2. Attraction force

Bubbles on the horizontally placed hydrophobic surface, whose size was close to that which resulted in detachment, were not vertically elongated but rather spherical in shape (Fig. 2). Therefore the volume of a bubble (spherical assumption yields the upper limit) on detachment is calculated as: $(4/3)\pi \times 2.1^3 = 38.8\ mm^3$. The calculated attachment force on detachment is the weight of the displaced water (where a 3 cm water column has a negligible effect): 3.9×10^{-5} kg = 38×10^{-5} N for both UW- and SP-wafers placed horizontally. There was no difference in diameter on tangential detachment from UW- and SP-wafers (3.3 and 3.5 mm, respectively), and therefore the mean tangential force on detachment was 20×10^{-5} N. This finding may have consequences for the size of bubbles on detachment from the inner wall of a blood vessel during and after decompression. The shear force applied to a bubble by blood flow increases while the bubble is growing, until equality of forces (blood-applied and tangential attachment) is reached and detachment occurs. Therefore, bubble volume on detachment will be related to blood flow in the different vessels. Because bubbles detach at a defined volume, time of detachment was therefore related to the growth rate of the bubbles, and ranged mainly from 0.5 to 3 h (Fig. 6). This time frame is similar to the crucial period for the risk of DCS in divers. The main initial occurrence of DCS was manifested during decompression (which was more extended than the fast decompression phase in the present study) and in the first 3 h after decompression (Elliott and Kindwall, 1982; Rivera, 1964; Slark, 1962). However, DCS is affected not only by the bubbles themselves but also by factors that develop as a consequence, such as activated platelets, endothelial dysfunction, and microparticles. The period during which bubbles may be detected following decompression usually lasts up to 3 h (Blogg and Gennser, 2011), in agreement with the findings of the present study.

4.3. Time for formation of gas micronuclei

The minimal normobaric time until bubbles were detected was about 20 min, mainly due to low flow of the saturated water. No difference was observed in bubble density as normobaric time increased. This suggests a nucleation time below 20 min. There are meager data on nucleation time in the formation of gas micronuclei. Daniels et al. (1984) suggested a half-time of 8–10 h for recovery of gas micronuclei in the over-pressurized prawn. Prebreathing oxygen, which was suggested to reduce effective gas micronuclei (Arieli et al., 2002), was effective after 2.5 h in divers (Castagna et al., 2009). The shorter nucleation time in the present study may be related to the mechanism of nucleation in the reported studies, or to the pure hydrophobic surface in the present study compared with living tissue; whereas the contact angle of the wafers was ~100°, the contact angle measured by Hills (1992) for blood vessels was 70–80°.

4.4. Models for calculating diving tables

Recent models for calculating the risk of DCS have made use of various theoretical propositions for the dimensions and distribution of gas micronuclei (Flook, 2000; Hugon et al., 2011; Wienke, 1990), each model with its theoretical basis. The size distribution of micronuclei was inferred from filtered gelatin studies (Yount and Hoffman, 1986; Yount et al., 1979). The size distribution of particles

in gelatin may differ from micronuclei formed on a flat hydrophobic surface. Most probably the gas within particle in the gelatin was there before the dry gelatin was mixed with water, which does not correlate with gas micronuclei within the body. Other models assumed spherical micronuclei for the calculation of gas exchange (Hugon et al., 2011; Van Liew and Burkard, 1993; Yount et al., 1979). However, the nanobubbles formed on a hydrophobic surface are oval and flat in form with 100 nm curvature (Meyer et al., 2005; Singh et al., 2006; Stevens et al., 2005; Switkes and Ruberti, 2004; Tyrrell and Attard, 2001; Yang et al., 2007), and the evolving micronuclei may therefore initially be in the form of flat bubbles. In the present study, the density of gas micronuclei increased in a linear fashion (open circles 180–400 kPa and filled squares 200–300 kPa, Fig. 4) with elevation of pressure and gas dissolution, suggesting a new relationship between the density of gas micronuclei and saturation pressure. Density was also higher with the increase in hydrophobicity. Hugon et al. (2011) summarized a number of models which calculated bubble growth assuming a very low diffusion coefficient to account for the expansion rate. The findings of the present study, together with those of our preceding investigation (Arieli and Marmur, 2011), may help in the future to construct a new generation of more realistic decompression models by possibly establishing the main site of formation of gas micronuclei and their dynamics.

5. Conclusion

Gas micronuclei are formed on flat, hydrophobic surfaces. The density of effective gas micronuclei increases as hyperbaric pressure is raised from 5 to 25 msw, and may stabilize thereafter. The attraction force on the hydrophobic surface may keep the bubble there until it reaches the appropriate size for release. This new may help construct better diving tables in the future.

Acknowledgements

The authors thank Dr. D. Cwikel for preparation of the surfaces, and Mr. R. Lincoln for skillful editing of the manuscript. This study was supported in part by a grant from the IDF Medical Corps and the Israel MOD.

References

Arieli, R., Marmur, A., 2011. Decompression sickness bubbles: are gas micronuclei formed on a flat hydrophobic surface? Respiratory Physiology and Neurobiology 177, 19–23.

Arieli, Y., Arieli, R., Marx, A., 2002. Hyperbaric oxygen may reduce gas bubbles in decompressed prawns by eliminating gas nuclei. Journal of Applied Physiology 92, 2596–2599.

Arieli, Y., Katsenelson, K., Arieli, R., 2007. Bubble reduction after decompression in the prawn *Palaemon elegans* by pretreatment with hyperbaric oxygen. Undersea and Hyperbaric Medicine 34, 369–378.

Blogg, S.L., Gennser, M., 2011. The need for optimisation of post-dive ultrasound monitoring to properly evaluate the evolution of venous gas emboli. Diving and Hyperbaric Medicine 41, 139–146.

Castagna, O., Gempp, E., Blatteau, J.-E., 2009. Pre-dive normobaric oxygen reduces bubble formation in scuba divers. European Journal of Applied Physiology 106, 167–172.

Considine, R.F., Hayes, R.A., Horn, R.G., 1999. Forces measured between latex spheres in aqueous electrolyte: non-DLVO behavior and sensitivity to dissolved gas. Langmuir 15, 1657–1659.

Craig, V.S.J., 1996. Formation of micronuclei responsible for decompression sickness. Journal of Colloid and Interface Science 183, 260–268.

Daniels, S., Eastaugh, K.C., Paton, W.D.M., Smith, E.B., 1984. Micronuclei and bubble formation: a quantitative study using the common shrimp, *Crangon crangon*. In: Bachrach, A.J., Matzen, M.M. (Eds.), Underwater Physiology. VIII: Proceedings of the Eighth Symposium on Underwater Physiology. Undersea Medical Society, Bethesda, MD, pp. 147–157.

Eckenhoff, R.G., Olstad, C.S., Carrod, G., 1990. Human dose–response relationship for decompression and endogenous bubble formation. Journal of Applied Physiology 69, 914–918.

Elliott, D.H., Kindwall, E.P., 1982. Manifestations of the decompression disorders. In: Bennett, P.B., Elliott, D.H. (Eds.), The Physiology and Medicine of Diving. , 3rd ed. Best Publishing Co., San Pedro, CA, pp. 461–472.

Flook, V., 2000. The physics and physiology of decompression. European Journal of Underwater and Hyperbaric Medicine 1, 1–8.

Fox, F.E., Herzfeld, K.F., 1954. Gas bubbles with organic skin as cavitation nuclei. Journal of the Acoustical Society of America 26, 984–989.

Harvey, E.N., Barnes, D.K., McElroy, W.D., Whiteley, A.H., Pease, D.C., Cooper, K.W., 1944. Bubble formation in animals. I: physical factors. Journal of Cellular and Comparative Physiology 24, 1–22.

Hayward, A.T.J., 1967. Tribonucleation of bubbles. British Journal of Applied Physics 18, 641–644.

Hennessy, T.R., 1989. On the site of origin, evolution and effects of decompression microbubbles. In: Brubakk, A.O., Hemmingsen, B.B., Sundnes, G. (Eds.), Supersaturation and Bubble Formation in Fluids and Organisms: An International Symposium. Kongsvoll, Norway, 6–10 June 1988. Tapir Publishers, Trondheim, Norway, pp. 292–332.

Hills, B.A., 1992. A hydrophobic oligolamellar lining to the vascular lumen in some organs. Undersea Biomedical Research 19, 107–120.

Hugon, J., Rostain, J.-C., Gardette, B., 2011. A new biophysical decompression model for estimating the risk of articular bends during and after decompression. Journal of Theoretical Biology 283, 168–179.

Jones, A.D., Miller, B.G., Colvin, A.P., 2007. Evaluation of Doppler Monitoring for the Control of Hyperbaric Exposure in Tunnelling. Health and Safety Executive, Bootle, Merseyside, UK, Appendix 2, pp. 115–120 (HSE Research Report RR598) http://www.hse.gov.uk/research/rrhtm/rr598.htm (accessed 14.02.12).

Liebermann, L., 1957. Air bubbles in water. Journal of Applied Physics 28, 205–211.

Meyer, E.E., Lin, Q., Israelachvili, J.N., 2005. Effects of dissolved gas on the hydrophobic attraction between surfactant-coated surfaces. Langmuir 21, 256–259.

Rivera, J.C., 1964. Decompression sickness among divers: an analysis of 935 cases. Military Medicine 129, 314–334.

Singh, S., Houston, J., van Swol, F., Brinker, C.J., 2006. Superhydrophobicity: drying transition of confined water. Nature 442, 526.

Slark, A.G., 1962. Treatment of 137 Cases of Decompression Sickness. Medical Research Council, Royal Naval Personnel Research Committee, Royal Naval Physiological Laboratory, London, UK (RNPL Report 8/62).

Seddon, J.R.T, Zandvliet, H.J.W., Lohse, D., 2011. Knudsen gas provides nanobubble stability. Physical Review Letters 107, 116101-1–116101-4.

Stevens, H., Considine, R.F., Drummond, C.J., Hayes, R.A., Attard, P., 2005. Effects of degassing on the long-range attractive force between hydrophobic surfaces in water. Langmuir 21, 6399–6405.

Switkes, M., Ruberti, J.W., 2004. Rapid cryofixation/freeze fracture for the study of nanobubbles at solid–liquid interfaces. Applied Physics Letters 84, 4759–4761.

Tyrrell, J.W.G., Attard, P., 2001. Images of nanobubbles on hydrophobic surfaces and their interactions. Physical Review Letters 87, 176104.

Van Liew, H.D., Burkard, M.E., 1993. Density of decompression bubbles and competition for gas among bubbles, tissue, and blood. Journal of Applied Physiology 75, 2293–2301.

Weijs, J.H., Snoeijer, J.H., Lohse, D., 2012. Formation of surface nanobubbles and the universality of their contact angles: a molecular dynamics approach. Physical Review Letters 108, 104501-1–104501-6.

Wienke, B.R., 1990. Reduced gradient bubble model. International Journal of Bio-Medical Computing 26, 237–256.

Yang, S., Dammer, S.M., Bremond, N., Zandvliet, H.J.W., Kooij, E.S., Lohse, D., 2007. Characterization of nanobubbles on hydrophobic surfaces in water. Langmuir 23, 7072–7077.

Yount, D.E., Hoffman, D.C., 1986. On the use of a bubble formation model to calculate diving tables. Aviation Space and Environmental Medicine 57, 149–156.

Yount, D.E., Strauss, R.H., 1976. Bubble formation in gelatin: a model for decompression sickness. Journal of Applied Physics 47, 5081–5089.

Yount, D.E., Kunkle, T.D., D'Arrigo, J.S., Ingle, F.W., Yeung, C.M., Beckman, E.L., 1977. Stabilization of gas cavitation nuclei by surface-active compounds. Aviation Space and Environmental Medicine 48, 185–191.

Yount, D.E., Yeung, C.M., Ingle, F.W., 1979. Determination of the radii of gas cavitation nuclei by filtering gelatin. Journal of the Acoustical Society of America 65, 1440–1450.